Electronic Supplementary Material (ESI) for Nanoscale Advances.

Supporting Information: Controlling the Rotation Modes of Hematite Nanospindles by Dynamic Magnetic Fields

Dirk Honecker,[†] Philipp Bender,[‡] Yannic Falke,[¶] Dominique Dresen,[¶] Matthias Kundt,[¶] Annette M. Schmidt,[¶] Andreas Tschöpe,[§] Michael Sztucki,[‖] Manfred Burghammer,[‖] and Sabrina Disch*,[¶]

†*ISIS Neutron and Muon Facility, Rutherford Appleton Laboratory, Didcot, OX11 0QX,UK*

‡*Heinz Maier-Leibnitz Zentrum (MLZ), Technische Universität München, Lichtenbergstraße 1, 85748 Garching, Germany*

¶*Department für Chemie, Universität zu Köln, Greinstr. 4-6, 50939 Köln, Germany*

§*Experimentalphysik, Universität des Saarlandes, Saarbrücken, Germany*

‖*European Synchrotron Radiation Facility (ESRF), F-38043 Grenoble, France*

E-mail: sabrina.disch@uni-koeln.de

S1 Synthesis

The hematite nanospindles were synthesized according to Matijević and co-workers.[1] In brief, aqueous solutions of 6.4875 g $FeCl_3 \cdot 6\,H_2O$ (24 mmol) and 0.0858 g $NaH_2PO_4 \cdot H_2O$ (0.72 mmol) were combined in synthetic water at a temperature of 85°C. The solution was stirred under reflux conditions for 48h and then rapidly cooled to room temperature. The obtained nanoparticles were separated from the solvent by centrifugation and redispersed by sonication into synthetic water, a procedure that was repeated five times. The obtained nanoparticles were further electrostatically stabilized using citric acid according to Wagner et al.[2]

S2 Characterization

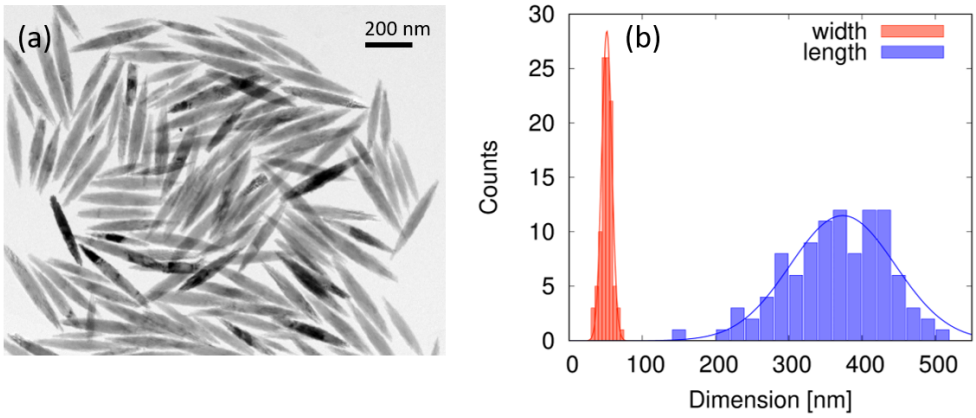

Figure S1: a) TEM image of the hematite nanospindles. b) Spindle diameter (orange) and length (blue) measured manually from 100 individual particles (histogram) with refinement of a lognormal size distribution (solid lines).

S2.1 Transmission Electron Microscopy (TEM)

The nanoparticles were drop-casted from diluted aqueous dispersion onto a coated copper grid for TEM with a Zeiss LEO 902 operated at 120 kV. Particle size histograms were obtained by manual evaluation of the spindle length and diameter for at least 100 particles.

The mean size and size distribution were obtained be fitting a normal distribution function to the obtained histograms.

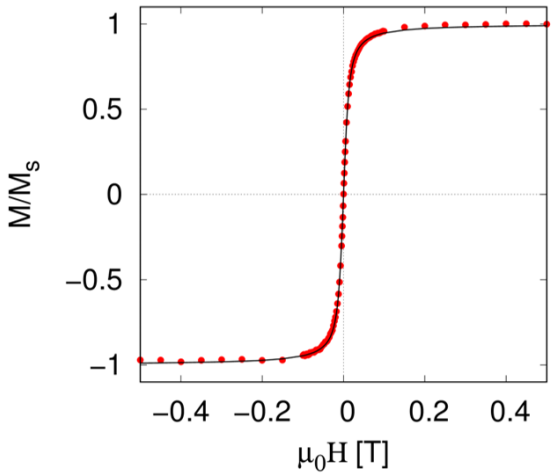

Figure S2: Macroscopic magnetization measurement (points), refined according to the Langevin behavior (solid line).

S2.2 Vibrating Sample Magnetization (VSM)

Quasi-static magnetization measurements were carried out on an ADE Magnetics VSM EV7. The dilute nanoparticle dispersion was sealed in a Teflon crucible, and field dependent magnetization data was collected at 298 K in a magnetic field range up to 2.2 T. The data shown in Fig. S2 was corrected for excess paramagnetic susceptibility observed at high magnetic field and fitted according to the modified Langevin equation $M/M_\mathrm{s} = L(\xi) = (\coth \xi - \frac{1}{\xi})$, where $\xi = \frac{\mu\mu_0 H}{k_\mathrm{B}T}$ is the Langevin parameter with the permeability of free space of μ_0, the integrated particle moment of μ, the Boltzmann constant k_B and the temperature T. The integrated particle moment is related to the spontaneous magnetization and particle volume according to $\mu = M_\mathrm{s}V$.

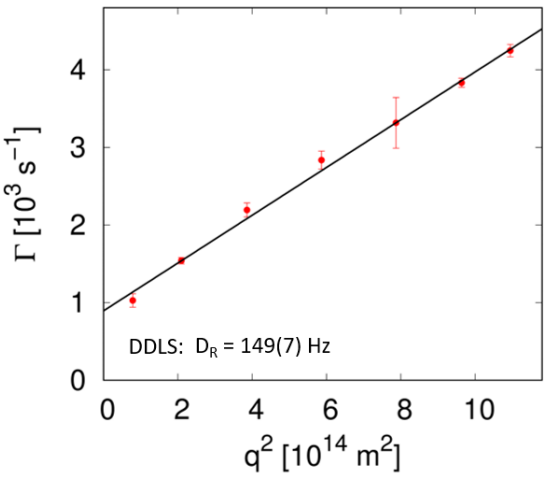

Figure S3: Depolarized DLS data.

S2.3 Depolarized Dynamic Light Scattering (DDLS)

The DDLS setup consisted of a laboratory built goniometer equipped with an Ar^+ laser (λ = 488 nm), a fiber optical detector, and an ALV autocorrelator. The typical laser power was 15 mW. Measurements were carried out at 298 K using 10 mm cylindrical cuvettes (VWR) immersed into a thermostated index matching bath (toluene, ± 0.1 K). For depolarized dynamic light scattering measurements, the primary beam and the scattered light passed through Glan–Thompson polarizers. The measured depolarised correlation function allows to extract the relaxation rate Γ measured at various angles 2θ corresponding to a range of wave vector $q = \frac{4\pi n}{\lambda}\sin(\theta)$, with n the refractive index. For a dilute dispersion without interactions, linear extrapolation with the relaxation rate $\Gamma = D_{\mathrm{T}}q^2 + 6D_{\mathrm{R}}$ provides the translational and rotational diffusion constants D_{T} and D_{R}.[3] The diffusion constants are sensitive to experimental parameters including the temperature and viscosity η of the solvent and the dimensions of the studied particles. The rotational diffusion coefficient is related to the rotational friction according ξ_{r} to the relation $D_{\mathrm{R}} = k_{\mathrm{B}}T/\xi_{\mathrm{r}}$, and can be estimated for a spherical particle with hydrodynamic radius R_{h} according to $D_{\mathrm{R}} = k_{\mathrm{B}}T/8\pi R_{\mathrm{h}}^3\eta$. For an ellipsoid of revolution with long half axis a and minor half axis b, the rotational friction for rotation around the minor axis is given as $\xi_{\mathrm{r}} = \frac{32}{3}\pi\eta\frac{a^4-b^4}{(2a^2-b^2)S-2a}$ with $S = \frac{2}{\sqrt{a^2-b^2}}\log(\frac{a+\sqrt{a^2-b^2}}{b})$.[4]

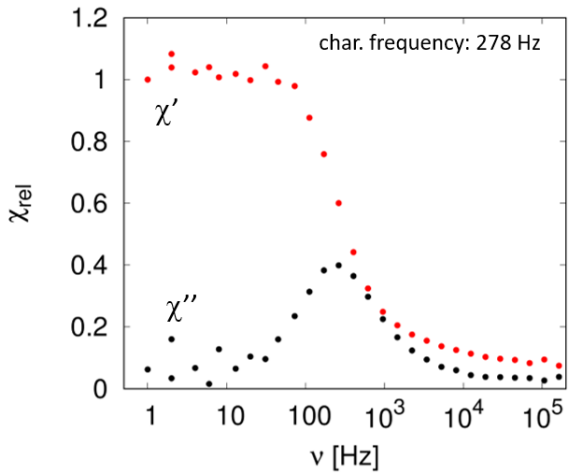

Figure S4: AC magnetic susceptrometry data.

S2.4 AC Magnetic Susceptometry (ACMS)

AC magnetization data was acquired using an Imego DynoMag Susceptometer. The real and imaginary parts of the magnetic susceptibility were measured at 298 K in an alternating magnetic field of $\mu_0 H = 0.5$ mT in a frequency range of 0.1 Hz – 10 kHz. AC susceptiblity probes the magnetic dynamics of relatively slow processes. If the field frequency coincides with typical relaxation timescales in the system, the occuring dissipation is reflected in a maximum of the imaginary magnetic susceptibility.[5]

S2.5 Optical Transmission

The custom-built setup consisted of a HeNe laser ($\lambda = 632.8$ nm), a Helmholtz coil set, and a Thorlab DET36A/M photodetector.[6] The nanoparticle dispersion was measured using a 10 mm × 10 mm cuvette placed in the center of a set of Helmholtz coils very similar to those used for the stroboscopic SAXS experiment. The individual Helmholtz coils are driven by an AC sine signal with a 90° phase shift to generate an overall rotating magnetic field with 10 mT field amplitude and frequencies up to 600 Hz.

S3 Stroboscopic SAXS

Time-resolved SAXS measurements were carried out using the ID13 instrument (ESRF) at 13 keV ($\lambda = 0.9537$ Å). A custom magnetic field setup consisting of two crossed Helmholtz coil-sets[7] was installed at the sample position. Alternating magnetic fields oriented perpendicular and parallel to the X-ray beam were generated with a resonance circuit consisting of a frequency generator (Agilent 6642A) and an audio amplifier (Crown XLS5000). To match the impedance of the coils at high frequencies, a variable number of capacities connected to a 100 pin terminal block (Agilent U2903A) could be connected in series by means of a Digital I/O (Agilent U2653A). For a rotating magnetic field, both coil-sets were driven with the same frequency but $\pi/2$ phase shift. Rotating and alternating magnetic field frequencies were accessible in the range of 25 Hz - 1000 Hz. Due to the large impedance, the custom-made Helmholtz coil set had a maximal magnetic field of 10 mT at the highest frequencies. For higher magnetic fields, we observed significant heat dissipation from the magnetic coils."

The aqueous dispersion of nanospindles was sealed in a quartz capillary and mounted in the center of the Helmholtz coil-sets. The Maxipix 2x2 four-element pixel detector (516 x 516 pixels/frame with 55 x 55 μm^2 pixel size and 350 Hz max. frame rate) used for this experiment was set up at 1.787 m distance from the sample position. For time-resolved measurements up to a dynamic magnetic field frequency of 300 Hz, the magnetic field period was separated into 20 time frames, and the detector gating with respect to the magnetic field phase was set up to collect the scattering data in the individual time frames with 0.1 s exposure time per frame. Time-integrated SAXS measurements were carried out by continuous data acquisition.

S3.1 Static SAXS

Time-integrated SAXS data acquired in zero field condition was corrected for the scattering contribution of the empty capillary and the pure solvent. The data was azimuthally averaged

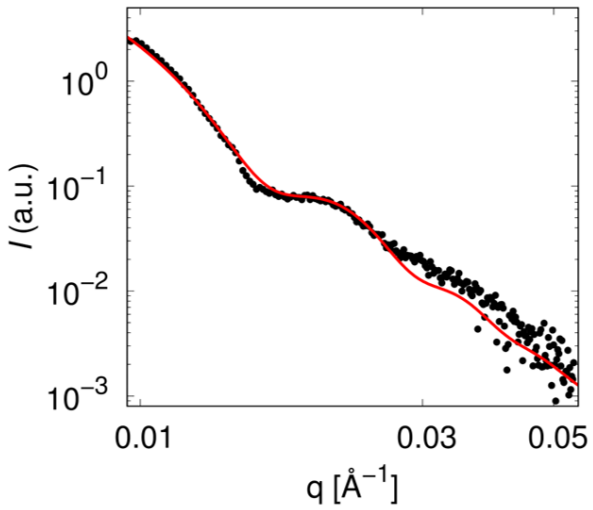

Figure S5: Isotropic SAXS data in zero magnetic field (points) with fit of ellipsoidal form factor (red line).

and analyzed using the form factor of an ellipsoid of revolution, revealing a spindle diameter of 49.9 nm with an intermediate lognormal size distribution of 9.6%. Because the particle length is not accessible within the given q-range, it was fixed to the TEM result.

S3.2 Data treatment

All measurements were performed in dynamic field (Fig. S6a) and then repeated in zero field (Fig. S6b). The intensity difference between the SAXS measured in applied field and in zero field condition (Fig. S6c) is shown to emphasize the scattering anisotropy indicating the orientation distribution of the nanospindles. In addition, the transmission of the direct beam through the beam stop is masked in the difference pattern, leaving only the sample-related differential scattering intensity.

The full period of the stroboscopic SAXS results in alternating and rotating magnetic field of 25 Hz is shown in Fig. S7. For the isotropic, but negative SAXS difference images found for the rotating case at at the $1/2\ \pi$ and $3/2\ \pi$ time frames, the underlying individual scattering intensities in applied field and isotropic conditions, corrected for the scattering background of the empty capillary) are given in Fig. S8.

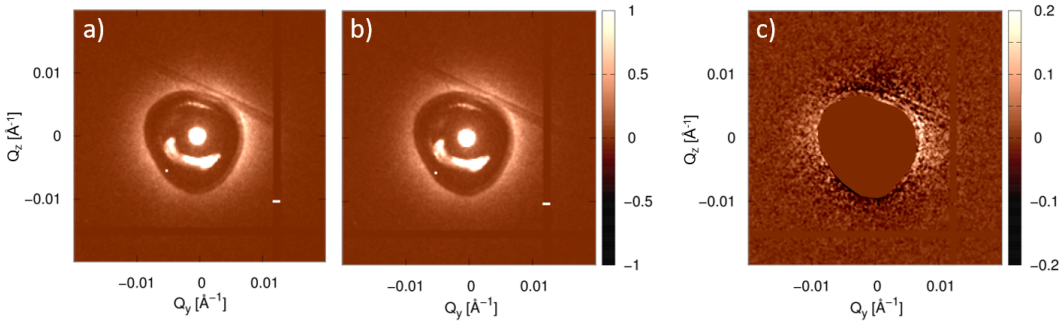

Figure S6: SAXS detector images a) Anisotropic scattering intensity in a selected time frame with 10 mT applied magnetic field. b) Isotropic scattering intensity in zero field. c) Difference between (a) and (b) with masked beam stop.

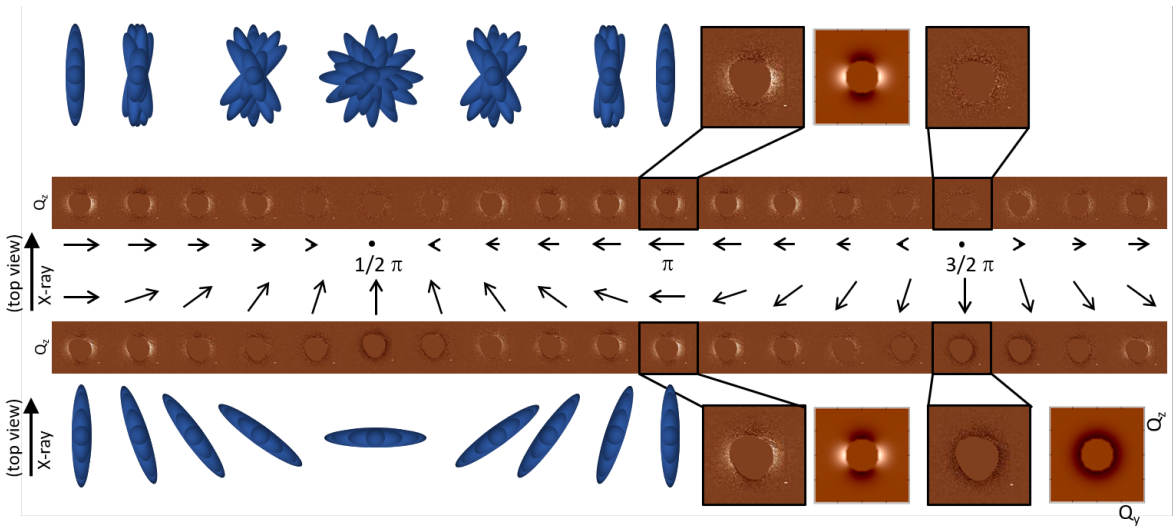

Figure S7: Stroboscopic SAXS by hematite nanospindles in alternating (top) and rotating (bottom) magnetic fields of 25 Hz. The field configuration is depicted by black arrows (center) next to the SAXS difference images for an entire period (0 - 2 π). The average, time-resolved nanospindle orientation is depicted schematically. For comparison, the computed scattering patterns according to the expected orientation of the nanospindle ensemble are shown for selected time frames in alternating and rotating field.

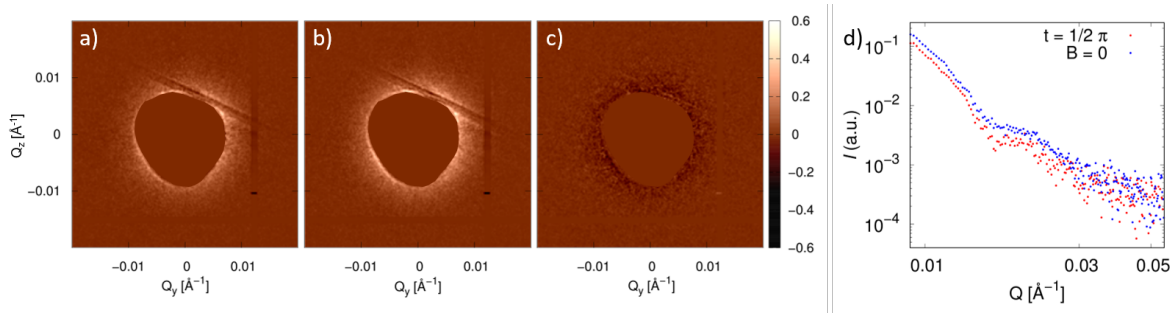

Figure S8: Stroboscopic SAXS by hematite nanospindles in rotating magnetic field of 25 Hz. a) Scattering intensity in the $1/2\ \pi$ and $3/2\ \pi$ time frame with applied field. b) Isotropic scattering in zero field (reference measurement). c) Difference between (a) and (b). Beam stop is masked in all patterns. d) Azimuthally integrated scattering intensities for both cases ((a) in red and (b) in blue).

S3.3 Scattering Anisotropy

The scattering anisotropy is determined from the horizontal and vertical scattering intensities radially integrated in a q range of 0.01 - 0.015 Å^{-1} and derived as the difference between maximum and minimum differential scattering intensities. Despite not being directly related to an order parameter, this parameter gives a quantitative impression of the degree of nanospindle alignment.

S3.4 Orientation Distribution

Computed scattering patterns are based on the orientation distribution of the nanospindles as introduced in Zákutná et al.[8]. In the scattering model, the long axis of the form factor of an ellipsoid or revolution is oriented perpendicular to the easy axis that precesses around the applied field direction with Boltzmann statistics. The angular distribution $P(\psi)$ of the easy axis towards the applied magnetic field direction follows Boltzmann statistics

$$P(\psi) = \frac{\xi \exp\left(\xi \cos(\psi)\right)}{\exp\left(\xi - 1\right)} \tag{1}$$

with the Langevin parameter $\xi = \frac{\mu \mu_0 H}{k_B T}$, where μ is the integral moment of the nanospindles, $\mu_0 H$ is the applied magnetic field, k_B is the Boltzmann constant, and T is the temperature.

The model is available in the Sasview Model Marketplace as 'Magnetically oriented, rotating and precessing anisometric particle (MORP)'.[9]

To simulate the scattering patterns of the individual time frames, either the applied magnetic field strength (alternating case) or the field direction (rotating case) of the SAXS model was integrated according to the range of the field condition in the particular time frame.

For the time-averaged SAXS in 300 Hz alternating field, the orientation distribution of the nanospindles in a 10 mT applied magnetic field is computed ($\xi = 1.85$).

For the time-averaged SAXS in 300 Hz rotating field, we model a collinear orientation of the long spindle axis towards the direction perpendicular to the rotation plane, following again Boltzmann statistics. The computed scattering pattern shown in the main manuscript was derived using an intermediate Langevin parameter of $\xi = 1$.

References

(1) Ozaki, M.; Kratohvil, S.; Matijević, E. Formation of Monodispersed Spindle-Type Hematite Particles. *Journal of Colloid and Interface Science* **1984**, *102*, 146–151.

(2) Wagner, J.; Autenrieth, T.; Hempelmann, R. Core Shell Particles Consisting of Cobalt Ferrite and Silica as Model Ferrofluids [CoFe2O4–SiO2 Core Shell Particles]. *Journal of Magnetism and Magnetic Materials* **2002**, *252*, 4–6.

(3) Glidden, M.; Muschol, M. Characterizing Gold Nanorods in Solution Using Depolarized Dynamic Light Scattering. *The Journal of Physical Chemistry C* **2012**, *116*, 8128–8137.

(4) Perrin, F. Brownian motion of an ellipsoid - I. Dielectric dispersion for ellipsoidal molecules. *J. Phys. Radium* **1934**, *5*, 497 – 511.

(5) Topping, C. V.; Blundell, S. J. A.C. susceptibility as a probe of low-frequency magnetic dynamics. *Journal of Physics: Condensed Matter* **2018**, *31*, 013001.

(6) Günther, A.; Bender, P.; Tschöpe, A.; Birringer, R. Rotational Diffusion of Magnetic Nickel Nanorods in Colloidal Dispersions. *J. Phys.: Condens. Matter* **2011**, *23*, 325103.

(7) Bender, P.; Günther, A.; Honecker, D.; Wiedenmann, A.; Disch, S.; Tschöpe, A.; Michels, A.; Birringer, R. Excitation of Ni Nanorod Colloids in Oscillating Magnetic Fields: A New Approach for Nanosensing Investigated by TISANE. *Nanoscale* **2015**, *7*, 17122–17130.

(8) Zákutná, D.; Falke, Y.; Dresen, D.; Prévost, S.; Bender, P.; Honecker, D.; Disch, S. Morphological and Crystallographic Orientation of Hematite Spindles in an Applied Magnetic Field. *Nanoscale* **2019**, *11*, 7149–7156.

(9) Dresen, D. Magnetically oriented, rotating and precessing ellipsoid model. `http://marketplace.sasview.org/models/133/`, (accessed January 28, 2022).